

Tunable thermal conductivity in silicon twinning superlattice nanowiresShiyun Xiong,^{1,2} Yuriy A. Kosevich,^{1,2,3} K. Säskilähti,^{1,2,4} Yuxiang Ni,^{1,2,*} and Sebastian Volz^{1,2,†}¹*CNRS, UPR 288 Laboratoire d'Energétique Moléculaire et Macroscopique, Combustion (EM2C), Grande Voie des Vignes, 92295 Châtenay-Malabry, France*²*Ecole Centrale Paris, Grande Voie des Vignes, 92295 Châtenay-Malabry, France*³*Semenov Institute of Chemical Physics, Russian Academy of Sciences, 119991 Moscow, Russia*⁴*Department of Biomedical Engineering and Computational Science, Aalto University, FI-00076 Aalto, Finland*
(Received 17 September 2014; revised manuscript received 29 October 2014; published 24 November 2014)

Using nonequilibrium molecular dynamic simulations, the thermal conductivity of a set of Si phononic metamaterial nanowires with a twinning superlattice structure has been investigated. We first show that this latter structural modulation can yield 65% thermal-conductivity reduction compared to the straight wire case at room temperature. Second, a purely geometry-induced minimal thermal conductivity of the phononic metamaterial is observed at a specific period depending on the nanowire diameter. Mode analysis reveals that the minimal thermal conductivity arises due to the disappearance of favored atom polarization directions. The current thermal-conductivity reduction mechanism can collaborate with the other known reduction mechanisms, such as the one related to coating, to further reduce thermal conductivity of the metamaterial. Current studies reveal that twinning superlattice nanowires could serve as a promising candidate for efficient thermoelectric conversion benefitting from the large suppression in thermal transport and without deterioration of electron-transport properties when the surface atoms are passivated.

DOI: [10.1103/PhysRevB.90.195439](https://doi.org/10.1103/PhysRevB.90.195439)

PACS number(s): 65.80.-g, 44.10.+i, 63.20.-e

I. INTRODUCTION

Thermoelectric material, which can convert heat into electric power and vice versa, is one of the promising candidates for energy harvesting. The dimensionless figure of merit ZT , measuring the conversion efficiency, depends on the electrical conductivity, the Seebeck coefficient, and the thermal conductivity (κ). Due to its abundance in nature, to the sum of knowledge accumulated on its properties, and also to its environment friendly features, silicon has been extensively studied as a thermoelectric material and $ZT = 1$ has been achieved for Si nanowires (NWs) [1], a remarkable accomplishment in view of the poor thermoelectric conversion potential of the bulk counterpart. This significant progress in the figure of merit for Si is largely attributed to the remarkable reduction in thermal conductivity of Si NWs. Both experimental [1–5] and theoretical [5–13] works show that with the introduction of defects, such as surface roughness and heterogeneous coating, the thermal conductivity of Si NWs can be two orders of magnitude smaller than that of the crystalline bulk one. Although this significant achievement has been reached, it is still far from the desired efficiency of solid-state thermoelectric devices, where $ZT \sim 4$ is required [14]. Consequently, new mechanisms for κ reduction are greatly needed to reach the next milestone of Si thermoelectrics.

Heterostructure superlattices (SLs) are one kind of metamaterial that has been widely studied [15–20]. It has been shown that for a crystalline superlattice (SL), the cross-plane thermal conductivity can be one order of magnitude smaller than the one of bulk materials with a single component, and, in some cases, even smaller than the value of a random alloy with

the same elements due to the numerous interface scatterings. On the other hand, *geometric* (metamaterial) SLs composed of the same component have rarely been studied [21,22]. Nevertheless, SLs of this kind also have vital importance as they involve nontrivial consequences on the electronic and phonon properties of the materials.

Twinning, also known as the planar stacking fault, is one of the most important defects in materials science and it is most often related to mechanical properties [23,24]. Recent experiments [25–28] show that twin planes are commonly found in NWs with fcc structures grown in the $\langle 111 \rangle$ direction, e.g., InP, SiC, GaP, Si, etc. These twin planes are distributed periodically along the NWs and form a twinning SL NW. The diameter and period length of these metamaterial NWs can be controlled during the synthesis process, offering the degree of freedoms for tuning their properties. More interestingly, NWs with twinning SLs feature a zigzag arrangement of periodically twinned segments with a rather uniform thickness along the entire growth length, offering a mechanism for shape controlling during the growth of NWs. The impact of twinning on mechanical [23,24], electronic [29,30], and optical properties [30] has been widely studied, while this impact remains unexplored concerning thermal properties. Unlike heterostructure SLs with fundamental A and B units, where the units A and B differ either in local crystalline structure or local composition or both, the units A and B of a twinning SL exhibit the same local structure and composition and they differ only by a relative rotation of the crystal orientation, i.e., A and B are “twins” [27]. As a result, the conventional mechanisms for SL interface scattering, such as mass mismatch and lattice mismatch, are not applicable and alternative phonon scattering mechanisms taking place in twinning SLs should be investigated.

In this work, we perform nonequilibrium molecular dynamics (NEMD) simulations to calculate the thermal conductivity of the Si metamaterial NWs with twinning SLs. We show

*Present address: Department of Mechanical Engineering, University of Minnesota, Minneapolis, Minnesota 55455, USA.

†sebastian.volz@ecp.fr

that the thermal conductivity of the twinning SL NWs can be remarkably reduced up to 65% at room temperature compared to their pristine counterpart. A minimum thermal conductivity due to the geometric effect is found with a specific SL period, which is equal to 1/3 of the diameter.

II. STRUCTURE AND SIMULATION DETAILS

Figure 1 depicts the structure formation of the twinning SL with the diameter D and period L_p . For a close-packing structure, there are usually three types of stacking sites with exactly the same configuration but having a shift one from another in a specific direction. The three stacking sites are usually labeled as A , B , and C . The B and C sites can be obtained from the A site with a shift of $(1 + 3n)b_v$ and $(2 + 3n)b_v$, respectively, where b_v is the minimum shift length, as shown in Fig. 1(a), and n is an integer. The stacking sequence of $ABCABC$ in the $\langle 111 \rangle$ direction forms the fcc structure and the $ABABAB$ one forms the hcp structure. For Si having a fcc diamond lattice, the shift between different sites is along the $\langle 112 \rangle$ crystal orientation with $b_v = 2.217 \text{ \AA}$. The cross section of the wire is chosen as hexagonal with the diameter D , which is shown in Fig. 1(b). The wire first grows according to a fcc structure, i.e., following a stacking in the $ABCABC$ sequence with the same shift given by the vector b_v between the neighboring layers. After several ABC periods, a stacking fault is introduced, and instead of stacking an A layer, a B layer is directly introduced after the C layer with a shift of b_v in the opposite direction. After the stacking fault, the stacking sequence changes to $CBACBA$, which is purely symmetrical to the previous stacking, as is shown in Fig. 1(c). As a result, a kink is formed with the angle $\theta = 109.4^\circ$.

NEMD simulations are performed by using LAMMPS software [31] with the commonly adopted Stillinger-Weber

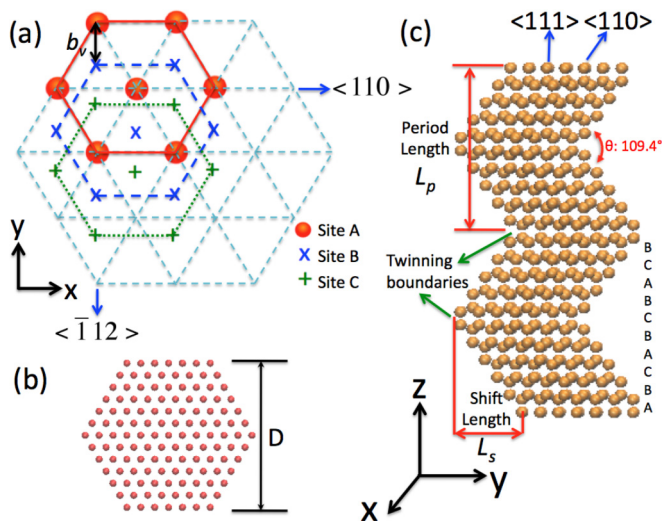


FIG. 1. (Color online) Schematic figure of the twinning SL stacking with diameter D and period length L_p . (a) Three possible stacking sites labeled with A , B , and C in closely packed structures. The three sites are identical but are shifted in the $\langle 112 \rangle$ direction one from another. (b) An example of a hexagon cross section with the diameter D of the twinning SL NWs. (c) Stacking sequence of a Si twinning SL NW.

potential [32,33] describing the interactions between atoms. The velocity Verlet algorithm with an integration time step of 0.8 fs is used to solve the equations of motion. All of the structures are fully relaxed at zero pressure and at target temperatures (NPT) for 4 ns and then moved to an NVE ensemble with fixed boundary conditions on atomic layers at the two ends. Next to those fixed layers, with the help of the Nosé-Hoover thermostat [34,35], several layers of atoms were coupled to a hot and a cold bath having temperatures $T_0 + \Delta/2$ and $T_0 - \Delta/2$, respectively, where $\Delta = 20 \text{ K}$ in all simulations. 5 ns runs were performed to reach the nonequilibrium steady state, and another 5 ns to time average the local temperature T and the microscopic heat flux j along the z direction. The thermal conductivity (TC) κ were then extracted from the Fourier's law, i.e., $\kappa = -j(dT/dz)^{-1}$. All of the NWs' thermal conductivities were measured with the same kink leg length of 34.5 nm. Note that all of the simulations are done with free surfaces, while in real situations, the dangling bonds on surfaces should be passivated by, for example, hydrogen atoms. However, the influence on the thermal conductivity of hydrogen atom passivation remains weak due to the reduced hydrogen mass [36]. Consequently, only silicon atoms were considered in our simulations.

III. RESULTS AND DISCUSSIONS

Figure 2(a) represents the thermal conductivities of the Si twinning SL NWs as a function of period L_p and specified diameter D at 300 K. The thermal conductivities of the pristine NWs having the same diameters and lengths are also calculated and are summarized in Table I. Note that the length-dependent thermal conductivity in nanostructures has been extensively reported [7,37,38]. In this study, we focus on the relative reduction of thermal conductivity by the twinning rather than the absolute value or the length effect on thermal conductivity. As a result, we fix the length of the simulated NWs to 34.5 nm and consider TC as a function of SL period, temperature, and diameter of the NWs.

As is shown in Fig. 2(a), the thermal conductivities of the NWs with twinning SL are largely decreased compared to the one of the pristine NW. The reduction rate is comparable to one of the facet engineered nanowires [39]. A first guess regarding the thermal-conductivity reduction may arise from two reasons, i.e., the zigzag geometric effect and the twinning boundary scattering. To check the relative contribution of these two aspects, we calculated the thermal conductivities of the bulk Si twinning SLs by applying periodic boundary conditions in the x and y directions and compared them with the one of the silicon bulk material. With the periodic boundary condition in the x and y directions, the geometric effect is eliminated and we can purely focus on the scattering by the twinning boundaries. Surprisingly, regardless of the number of boundaries, the results show no difference with the value of the perfect bulk, indicating no impact on heat transfer from the twinning boundaries. All of the thermal-conductivity reduction in the SL NWs hence arises from the induced geometric effect, i.e., from the zigzag configuration. This can actually be observed directly from the temperature profile (not shown) for both bulk materials and nanowire SLs, where no temperature jump is observable around the twinning boundaries. The

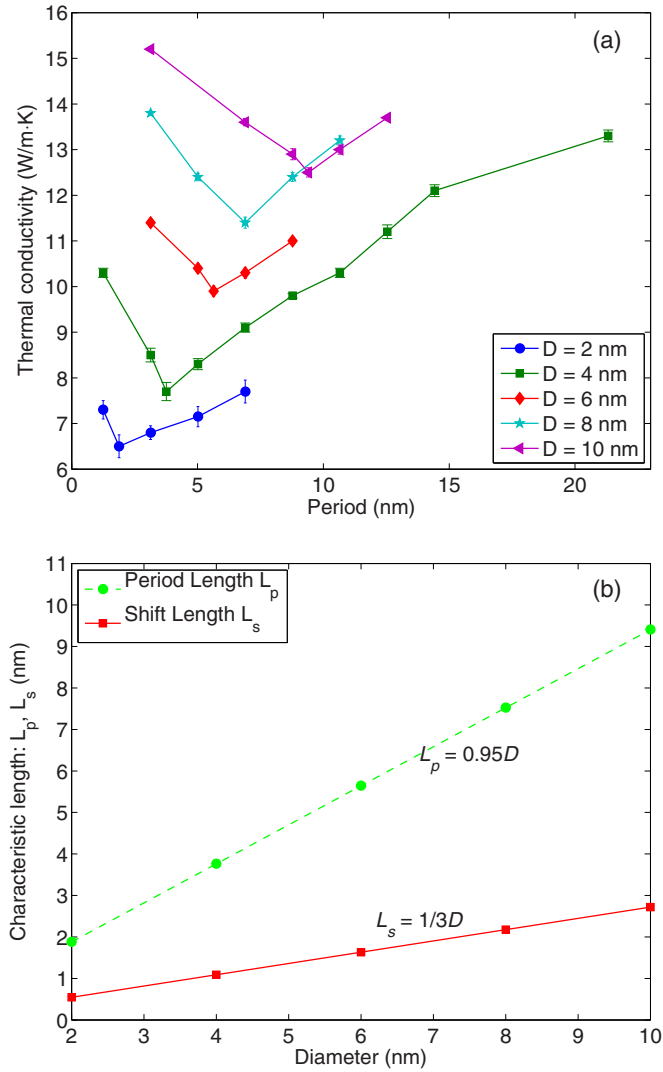


FIG. 2. (Color online) (a) Thermal conductivities of the twinning SL NWs as a function of the period for different diameters at 300 K. A minimum thermal conductivity appears at different period lengths for different diameters. (b) Period length L_p and shift length L_s corresponding to the minimum thermal conductivity vs the diameter. L_p and L_s are linked together with the relation $L_s = L_p/2 \times \cot(\theta/2)$.

reason may be found from the fact that each atomic layer is actually identical and the stacking sequence of $ABCACB$ and $ABCACB$ does not alter the force between the neighboring layers. Consequently, the atomic motion can be effectively transferred through the twinning boundaries.

When the diameter remains invariant, the increase in the SL period leads the thermal conductivity to decrease

TABLE I. Thermal conductivities of pristine NWs and twinning SL NWs with different diameters at 300 K. The resulting reductions in percentage are reported in the last line.

Diameter (nm)	2	4	6	8	10
Pristine NW κ (W/m K)	18.4 ± 0.15	19.4 ± 0.17	21.0 ± 0.10	22.7 ± 0.08	24.5 ± 0.11
SL minimum κ (W/m K)	6.5 ± 0.22	7.7 ± 0.20	9.9 ± 0.15	11.3 ± 0.10	12.5 ± 0.12
Maximum reduction (%)	64.7	60.3	53.0	50.0	49.0

first, reaching a minimum value, and then progressively to increase. The minimum thermal conductivity observed here seems similar to that observed in the heterostructure SLs [15–18]. However, the mechanism taking place in the twinning SL NWs completely differs from the one observed in heterostructure SL. In this latter situation, the minimum thermal conductivity is attributed to the interplay between the phonon coherence and the interface scattering. For the twinning SL NWs, the twinning boundary has no impact on heat transfer, and thermal-conductivity change is fully ascribed to the twinning-induced zigzag geometric effect as we discussed. This can be further confirmed from the diameter-dependent SL period corresponding to the minimum thermal conductivity, as displayed in Fig. 2(b). This figure clearly shows that the period length, corresponding to the minimal thermal conductivity, varies with the diameter according to the relationship $L_p = 0.95D$. In Fig. 1(c), we also defined the shift length L_s , representing the total length shift in the kink direction within one period. L_p and L_s are linked with a simple relation, i.e., $L_s = L_p/2 \times \cot(\theta/2)$ with $\theta = 109.4^\circ$. As a result, the L_s value corresponding to the minimal thermal conductivity is a function of the diameter and can be simply expressed as $L_s = D/3$, which is also shown in Fig. 2(b). It has been experimentally demonstrated that twinning boundaries have almost no effect on the electrical conductivity [40]. In twinning SL nanowires, electrical conductivity also remains at a high value in comparison with the one of the pristine structure if the surface atoms are passivated, for example, with hydrogen atoms [41]. As a result, the thermoelectric figure of merit of Si can be notably enhanced with the twinning SL NWs thanks to the significant thermal-conductivity decrease without significant deterioration of electron-transport properties.

To explain the large thermal-conductivity decrease as well as the minimal thermal conductivities, we performed the normal-mode polarization calculations. For a given mode λ , the α (x , y , or z) Cartesian component of a unit polarization vector $e_{i\alpha,\lambda}$ of an atom i is defined as [42]

$$e_{i\alpha,\lambda} = \frac{\varepsilon_{i\alpha,\lambda}}{\sum_{\alpha} \varepsilon_{i\alpha,\lambda}^* \varepsilon_{i\alpha,\lambda}}. \quad (1)$$

The normal-mode eigenvector components $\varepsilon_{i\alpha,\lambda}$ and their corresponding eigenfrequencies ω_λ are obtained by solving the lattice dynamics equation,

$$\omega_\lambda^2 \varepsilon_{i\alpha,\lambda} = \sum_{j\beta} \Phi_{i\alpha,j\beta} \varepsilon_{j\beta,\lambda}, \quad (2)$$

where $\Phi_{i\alpha,j\beta}$ is the harmonic force constant, which is calculated from the second derivative of the Stillinger-Weber potential used in MD simulations.

Figure 3 depicts the longitudinal acoustic (LA)-mode polarization vectors of each atom projected on the Y - Z

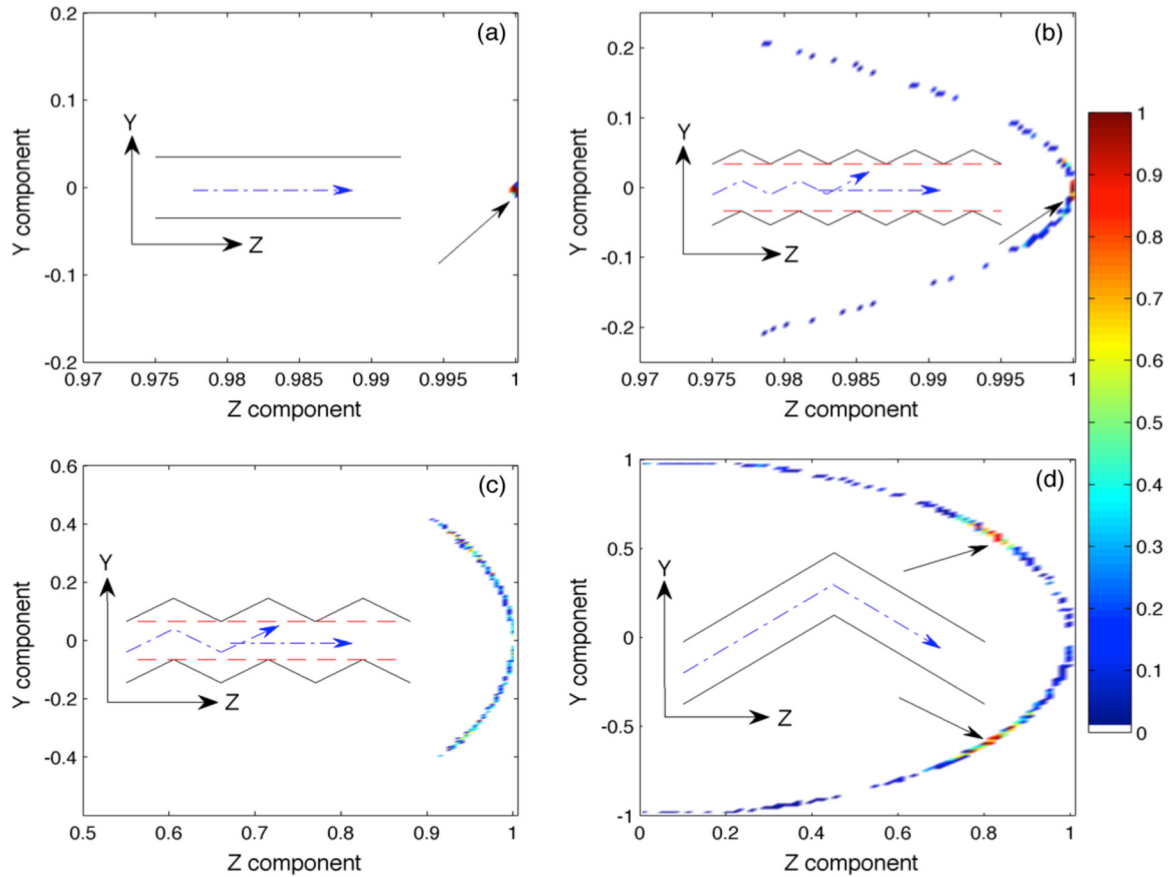


FIG. 3. (Color online) Y - Z components of the LA-mode vectors around the frequency 4.0 cm^{-1} for (a) the straight, (b) $L_p = 1.25 \text{ nm}$, (c) $L_p = 1.9 \text{ nm}$, and (d) $L_p = 10.6 \text{ nm}$ NWs with 2 nm in diameter. The color represents the number of modes and the maximum value has been normalized to 1. The corresponding structures are schematically indicated in each panel.

plane for the straight and the twinning SLs with different periods. The polarization vectors are calculated for the NWs of 2 nm in diameter and around the 4.0 cm^{-1} frequency. The corresponding structures are also schematically shown in each panel. For the straight NW, the normal modes possess well-defined polarization vectors, as indicated by the dashed arrow in Fig. 3(a), where all of the atoms show a unit polarization vector component near 1 in the z direction and almost zero in the x and y directions. This indicates that all of the atoms vibrate along the z direction. This is, of course, favorable for phonon transport. When the NW grows with twinning of small periods, the LA modes for some of the atoms start to have a small y component but still predominate in the z direction, as indicated by the arrow in Fig. 3(b). Those atoms with a small y component are typically the atoms around the kinks.

When the SL period increases to the length corresponding to the minimum thermal conductivity [Fig. 3(c)], the polarization vectors significantly broaden in the y direction and no clear preferential orientation appears. The polarization vectors homogeneously distributed on the arc range from -0.4 to 0.4 in the y direction and from 0.91 to 1.0 in the z direction. Atomic vibrations hence have scattered directions, yielding a hindered phonon transport and a decrease of the thermal conductivity compared to shorter period cases. With further elongation of the period, the atomic polarization vectors continue to broaden

in the y direction with a small fraction of interchanges between LA modes and transverse acoustic (TA) modes indicated by the y component near to the unity. This outcome agrees with the findings of Jiang *et al.* [9]. However, two preferred orientations of the polarization vectors can be clearly observed in Fig. 3(d), which for sure will increase the thermal conductivity compared to the homogeneously distributed cases. The two preferred orientations have their y and z components (y, z) around $(\pm 0.52, 0.81)$. It can be easily calculated that these two preferred directions are along the two legs of kink, respectively. It follows that most of the atoms vibrate along the two legs. It can be shown that the atoms having the two preferred directions are located in the middle of the legs. Those latter also contribute to 60%–70% of the atom polarization vectors for the NWs with $L_p = 10.6 \text{ nm}$. This percentage increases with the increase of period length, which agrees well with the increase of thermal conductivities when period length is increased beyond the minimum thermal-conductivity period.

Alternatively, the minimum thermal conductivities can be explained with a more intuitive geometric analysis. As shown in the structures of Fig. 3, phonons can propagate straightforwardly along the wire direction in the pristine NWs, leading to a thermal conductivity labeled as κ_s , which should be proportional to the cross-section area of the straight part. However, for the twinning SL NWs with long periods, phonons have to go along the legs, as shown by the dash-dotted arrow in

Fig. 3(d), in order to propagate from one side to the other side. The thermal conductivity resulting from this zigzag phonon propagation is labeled as κ_b . κ_b should be proportional to the period length and should saturate to κ_s when L_p is long enough. When the shift length L_s (defined in Fig. 1) is larger than the diameter, one has $\kappa_s = 0$ and the thermal conductivity of the wire is only composed of the heat flux involved in κ_b . However, in the cases when L_s is smaller than the diameter, phonons can propagate in both ways, as illustrated schematically by the arrows in Figs. 3(b) and 3(c), i.e., $\kappa = \kappa_s + \kappa_b$. Starting from $L_s = D$, with the decrease of period, κ_b decreases and κ_s increases from zero since the cross section of the straight part (noted by the red lines) enlarges progressively from zero. So there is a competition between κ_b and κ_s with the variation of the period, which finally results in the minimal thermal conductivity. This also interprets the diameter dependence of the minimum thermal conductivity as a function of period length. Therefore, the geometrical-period-dependent thermal

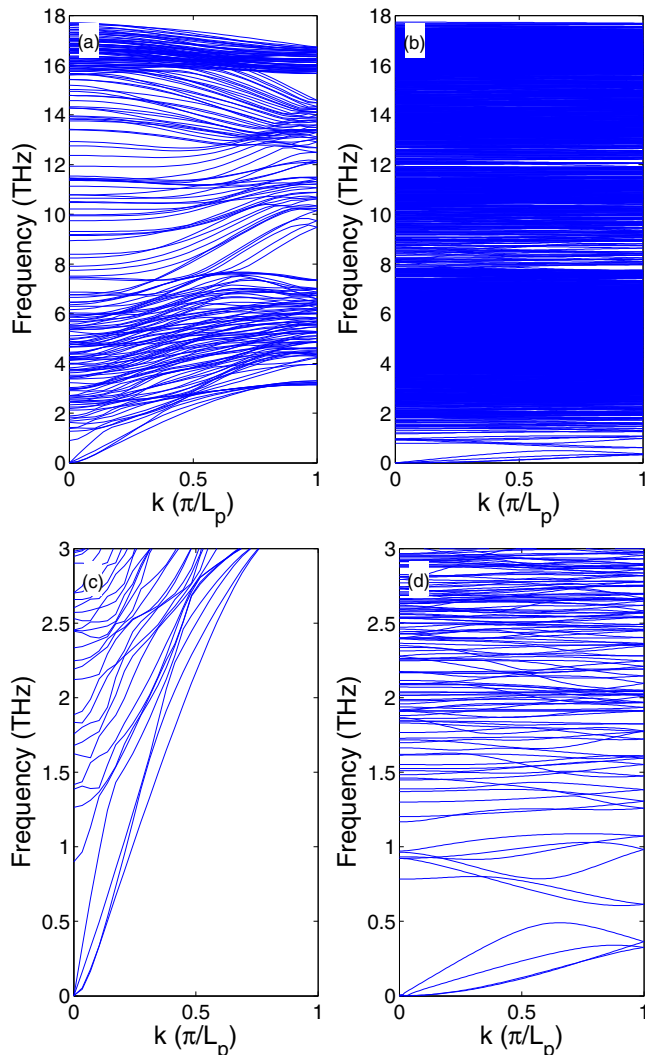


FIG. 4. (Color online) Phonon-dispersion relation of (a) the pristine NW with $D = 2$ nm and (b) the twinning SL phononic metamaterial NW with $L_p = 3.1$ nm, $D = 2$ nm; (c) and (d) are the corresponding $0 \leq \omega \leq 3$ THz of (a) and (b), respectively.

conductivity of twinning SLs enables the control of heat transport and thermoelectric conversion efficiency by changing only the geometric properties of such phononic metamaterials.

To know more about the vibrational properties of the twinning SL phononic metamaterial NW, we investigated the dispersion relation and compared it with that of pristine NWs (Fig. 4). The dispersion curve is calculated by solving the lattice dynamical equation [Eq. (2)] with the force constant matrix obtained from the LAMMPS software [31] based on the finite displacement method. The dispersion of both pristine and twinned NWs contains four acoustic branches, namely, one longitudinal, two transverse, and one torsion polarization branch. As the twinning SL NWs contain many more atoms in a period, their dispersion curve has many more branches. However, most of the branches are flat bands, giving smaller group velocities compared to the pristine structure. This is more clearly shown in the zoom-in plot in Figs. 4(c) and 4(d). More interestingly, the acoustic phonon frequency goes up to the optical phonon range, and no band gap between the acoustic and optical phonon branches is observed. However, for the twinning SL phononic NW with $L_p = 3.1$ nm, a small gap between the optical and acoustic branches appears, giving a phononic band-gap effect. The small group velocity of the twinning SL phononic metamaterial NWs hinders heat transfer, which can be identified more intuitively from the transmission function in Fig. 5 obtained from the Green's-function calculations [43].

As clearly shown in Fig. 5, the transmission function of the twinning SL NW with $L_p = 3.1$ nm is much smaller than the value of the pristine NW, although many more branches are contained in the twinning SL NWs, indicating a decrease of group velocity to a large extent. Especially for the phonons below 7 THz, the transmission is decreased by a factor of 3. Since the phonons in this frequency range carry most of the heat, the thermal transport in the twinning SL NWs is very hindered. The large group velocity suppression originates from the disappearance of a favored polarization direction and it is the immediate cause of thermal-conductivity reduction. The

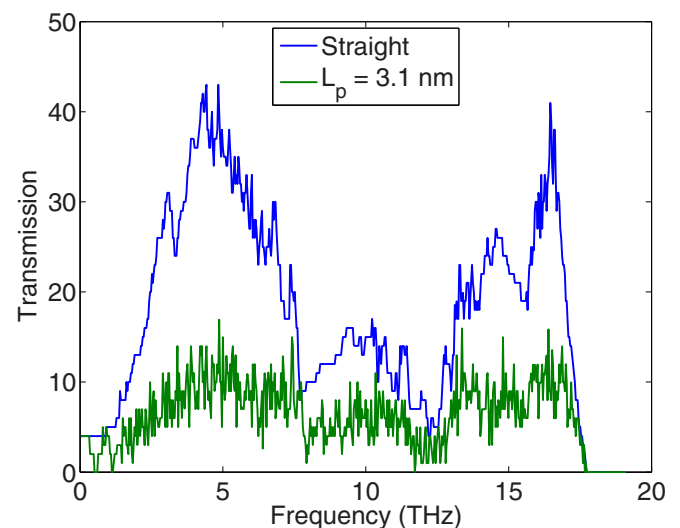


FIG. 5. (Color online) Phonon-transmission functions calculated with the phonon Green's function vary with the frequency.

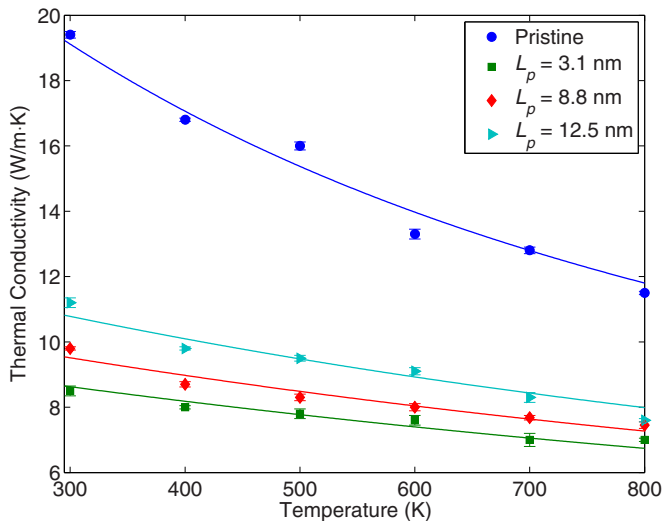


FIG. 6. (Color online) Temperature-dependent thermal conductivity of the pristine and twinning SL NWs with different periods and a diameter of 4 nm. The corresponding solid lines are fitted with Eq. (3).

transmission function also clearly shows the band gap between the acoustic and optical modes of the twinning SL NWs.

Figure 6 illustrates the temperature-dependent thermal conductivity of the pristine and twinning SL NWs of 4 nm in diameter and 34.5 nm in length. Due to the anharmonic effect, the thermal conductivity of the pristine NWs decreases quickly with the increase of temperature. However, for the twinning SL NWs, the thermal conductivities only decrease slightly when the temperature increases from 300 to 800 K, showing a weak dependence on the temperature. This trend appears because the phonon mean-free path in the twinning SL NWs is much smaller than in the pristine NWs and leads to weak temperature dependences for thermal conductivities in twinning SL NWs.

The phonon lifetime is commonly given by the Matheisen's rule, expressing the total inverse lifetime as the sum of the inverse lifetimes corresponding to each scattering mechanism. For the structures discussed here, only anharmonic and boundary scattering take place. Consequently, the total lifetime τ can be cast as $1/\tau = 1/\tau_b + 1/\tau_a$, where τ_b and τ_a are lifetimes of the boundary scattering and of the anharmonic scattering, respectively. The anharmonic scattering lifetime averaged over the frequency can be approximated as [44,45] $\tau_a^{-1} = BT e^{-C/T}$, with T being the absolute temperature, and $C = 137.3$ K and B are constants. Using the averaged specific-heat capacity C_v and the group velocity v_g , the relaxation time κ can be expressed as $\kappa = C_v v_g^2 \tau$. From this latter expression, it follows that $\kappa = C_v v_g^2 / (1/\tau_b + BT e^{-137.3/T})$. Let $a = \frac{1}{C_v v_g^2 \tau_b}$ and $b = \frac{B}{C_v v_g^2}$. Considering a and b as fitting parameters, the following equation can be used to fit the temperature-dependent thermal conductivities of different structures:

$$\kappa = \frac{1}{a + bT e^{-137.3/T}}. \quad (3)$$

In Fig. 6, the corresponding solid lines are fitted with Eq. (3). The temperature-dependent thermal conductivity κ

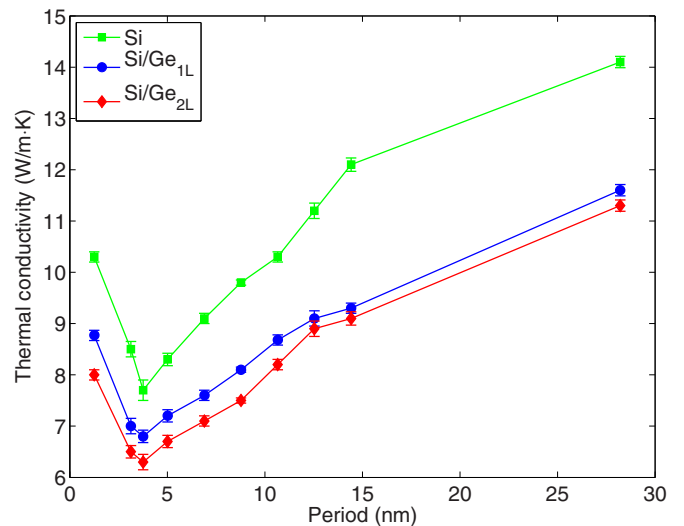


FIG. 7. (Color online) Thermal-conductivity variation with the twinning SL period for the Si and the Si-Ge core-shell structures with one- and two-atom-thick Ge atom layers. $D = 4$ nm for the pure Si NWs and the Si core in the core-shell NWs.

for all structures can be well fitted with the same constant $b = 6.7 \times 10^{-5}$, which characterizes the anharmonic effect. The parameter a related to the lifetime of the boundary scattering takes the values of 0.04, 0.08, 0.092, and 0.103 for the pristine and the twinning SLs corresponding to the periods 12.5, 8.8, and 3.1 nm, respectively. These values indicate a continuous decrease of the relaxation time due to boundary scattering for these structures.

To investigate whether the present thermal-conductivity reduction mechanism can collaborate with other well-known mechanisms, we coated Si twinning SL NWs ($D = 4$ nm) with one- or two-Ge-atom-thick layers, forming the core-shell twinning SL NWs. Mixed parameters for Si-Ge were based on the Stillinger-Weber potential according to Refs. [33,46].

The effect of the Ge atom coating on the thermal conductivities for the Si twinning SL NWs with different periods is illustrated in Fig. 7. As a comparison, the thermal conductivities of the Si twinning SL NWs without coating are also presented in the figure. Note that the diameters of the pure Si SL NWs and the Si core in the core-shell structures are the same. As can be seen from the figure, Ge coating still has a large impact on the thermal conductivities of Si twinning SL NWs, especially for small periods. With the Ge coating, the period corresponding to the minimum thermal conductivity does not change and the maximum reduction can reach almost 20% for only two atom layers of Ge coating. The thermal conductivity of the core-shell twinning SLs decreases with the increase of coating thickness at short periods while it almost does not change with coating thickness at large periods. The reduction of thermal conductivity by Ge coating is attributed to the increase of the boundary scattering rate, which further shortens the phonon mean-free path.

IV. CONCLUSIONS

The thermal conductivity of Si twinning SL phononic NWs has been investigated with different periods,

diameters, and temperatures by using NEMD simulations. It is demonstrated that the thermal conductivity can be reduced by 65% at room temperature compared to the straight NW case. Pure geometry-induced minimal thermal conductivity of the phononics is observed with the variation of the SL period. The corresponding periods are diameter dependent and almost equal to the diameter of the NW. A mode

analysis shows that the minimal thermal conductivity is due to the loss of preferential orientation of the polarization vectors induced by the kink. The considered mechanism of geometry-induced reduction of thermal conductivity in twinning superlattices can be complemented by other known mechanisms to further reduce thermal conductivity in phononic metamaterials.

-
- [1] A. I. Hochbaum, R. Chen, R. D. Delgado, W. Liang, E. C. Garnett, M. Najarian, A. Majumdar, and P. Yang, *Nature (London)* **451**, 163 (2008).
- [2] A. I. Boukai, Y. Bunimovich, J. Tahir-Kheli, J. K. Yu, W. A. Goddard, and J. R. Heath, *Nature (London)* **451**, 168 (2008).
- [3] D. Li, Y. Wu, P. Kim, L. Shi, P. Yang, and A. Majumdar, *Appl. Phys. Lett.* **83**, 2934 (2003).
- [4] S. K. Bux, R. G. Blair, P. K. Gogna, H. Lee, G. Chen, M. S. Dresselhaus, R. B. Kaner, and J. P. Fleurial, *Adv. Funct. Mater.* **19**, 2445 (2009).
- [5] P. Chen, N. A. Katcho, J. P. Feser, W. Li, M. Glaser, O. G. Schmidt, D. G. Cahill, N. Mingo, and A. Rastelli, *Phys. Rev. Lett.* **111**, 115901 (2013).
- [6] Y. He and G. Galli, *Phys. Rev. Lett.* **108**, 215901 (2012).
- [7] M. Hu and D. Poulikakos, *Nano Lett.* **12**, 5487 (2012).
- [8] S. G. Volz and G. Chen, *Appl. Phys. Lett.* **75**, 2056 (1999).
- [9] J. W. Jiang, N. Yang, B. S. Wang, and T. Rabczuk, *Nano Lett.* **13**, 1670 (2013).
- [10] J. Chen, G. Zhang, and B. Li, *Nano Lett.* **10**, 3978 (2010).
- [11] S. Xiong, J. Ma, S. Volz, and T. Dumitrica, *Small* **10**, 1756 (2014).
- [12] S. Volz and D. Lemonnier, *Phys. Low-Dimen. Str.* **5-6**, 91 (2000).
- [13] M. Kazan, G. Guisbiers, S. Pereira, M. R. Correia, P. Masri, A. Bruyant, S. Volz, and P. Royer, *J. Appl. Phys.* **107**, 083503 (2010).
- [14] A. T. M. Tritt, *Rev. Mater. Res.* **41**, 433 (2011).
- [15] P. Hyldgaard and G. D. Mahan, *Phys. Rev. B* **56**, 10754 (1997).
- [16] M. V. Simkin and G. D. Mahan, *Phys. Rev. Lett.* **84**, 927 (2000).
- [17] Y. K. Koh, Y. Cao, D. G. Cahill, and D. Jena, *Adv. Funct. Mater.* **19**, 610 (2009).
- [18] M. L. Lee and R. Venkatasubramanian, *Appl. Phys. Lett.* **92**, 053112 (2008).
- [19] S. Volz, J. Saulnier, G. Chen, and P. Beauchamp, *Microelectron. J.* **31**, 815 (2000).
- [20] A. Rajabpour and S. Volz, *J. Appl. Phys.* **108**, 094324 (2010).
- [21] K. Termentzidis, T. Barreateau, Y. Ni, S. Merabia, X. Zianni, Y. Chalopin, P. Chantrenne, and S. Volz, *Phys. Rev. B* **87**, 125410 (2013).
- [22] S. Merabia and K. Termentzidis, *Phys. Rev. B* **89**, 054309 (2014).
- [23] J. Wang and H. Huang, *Appl. Phys. Lett.* **88**, 203112 (2006).
- [24] Z. Lin, L. Wang, J. Zhang, X.-Y. Guo, W. Yang, H.-K. Mao, and Y. Zhao, *Scripta Mater.* **63**, 981 (2010).
- [25] F. J. Lopez, E. R. Hemesath, and L. J. Lauhon, *Nano Lett.* **9**, 2774 (2009).
- [26] P. E. Algra, M. A. Verheijen, M. T. Borgstrom, L. Feiner, G. Immink, W. J. P. van Enckevort, E. Vlieg, and E. P. A. M. Bakkers, *Nature (London)* **456**, 369 (2008).
- [27] Q. Xiong, J. Wang, and P. C. Eklund, *Nano Lett.* **6**, 2736 (2006).
- [28] D.-H. Wang, D. Xu, Q. Wang, Y.-J. Hao, G.-Q. Jin, X.-Y. Guo, and K. N. Tu, *Nanotechnology* **19**, 215602 (2008).
- [29] Z. Ikončić, G. P. Srivastava, and J. C. Inkson, *Phys. Rev. B* **48**, 17181 (1993).
- [30] Z. Ikončić, G. P. Srivastava, and J. C. Inkson, *Phys. Rev. B* **52**, 14078 (1995).
- [31] S. Plimpton, *J. Comput. Phys.* **117**, 1 (1995).
- [32] F. H. Stillinger and T. A. Weber, *Phys. Rev. B* **31**, 5262 (1985).
- [33] K. Ding and H. C. Andersen, *Phys. Rev. B* **34**, 6987 (1986).
- [34] S. Nosé, *Mol. Phys.* **52**, 255 (1984).
- [35] W. G. Hoover, *Phys. Rev. A* **31**, 1695 (1985).
- [36] H.-peng Li and R.-qin Zhang, *Europhys. Lett.* **105**, 56003 (2014).
- [37] C. W. Chang, D. Okawa, H. Garcia, A. Majumdar, and A. Zettl, *Phys. Rev. Lett.* **101**, 075903 (2008).
- [38] N. Yang, G. Zhang, and B. Li, *Nano Today* **5**, 85 (2010).
- [39] F. Sansoz, *Nano Lett.* **11**, 5378 (2011).
- [40] L. Lu, Y. Shen, X. Chen, L. Qian, and K. Lu, *Science* **304**, 422 (2004).
- [41] S. Zhong, T. Koch, M. Wang, T. Scherer, S. Walheim, H. Hahn, and T. Schimmel, *Small* **5**, 2265 (2009).
- [42] P. K. Schelling and S. R. Phillpot, *J. Amer. Ceramic Soc.* **84**, 2997 (2001).
- [43] N. Mingo and L. Yang, *Phys. Rev. B* **68**, 245406 (2003).
- [44] M. Asen-Palmer, K. Bartkowski, E. Gmelin, M. Cardona, A. P. Zhemov, A. V. Inyushkin, A. Taldenkov, V. Ozhogin, K. M. Itoh, and E. E. Haller, *Phys. Rev. B* **56**, 9431 (1997).
- [45] N. Mingo, *Phys. Rev. B* **68**, 113308 (2003).
- [46] S. Ethier and L. J. Lewis, *J. Mater. Res.* **7**, 2817 (1992).